Flexible Wiper System Dynamic Instabilities : Modelling and Experimental Validation

Carine Chevennement-Roux, Thomas Dreher, Patrick Alliot, Evelyne Aubry, Jean-Pierre Lainé, Louis Jézéquel

Flexible Wiper System Dynamic Instabilities: Modelling and Experimental Validation

C. Chevennement-Roux, **T. Dreher**, **P. Alliot**,
E. Aubry, **J.-P. Lainé**, **L. Jézéquel**

Abstract The optimization of wiper systems under various conditions and the creation of a product which is as robust as possible are the main objectives for an equipment supplier. However, in certain conditions, instabilities can appear and generate wiping defects due to the rubber-glass contact. To improve wiping quality and to reduce the number of test stages for design, this study proposes a wiper system modeling method. The wiper system is represented by a rigid blade holder on which a rubber blade is fitted. This rigid blade system is used on a flat test bench at constant wiping velocity. The model is based on modal synthesis methods and will be validated through comparison with experimental tests under various conditions. The right correlation obtained allows the same modelling method to be applied to the new generation of flexible wiper blades which take account of the degree of freedom of the wiper blade flexions. So, a new computation tool will be developed and validated through experimentation on a specific test bench.

Keywords Wiper systems · Instabilities · Vibration · Modelling · Friction · Hopf Bifurcation

C. Chevennement-Roux · T. Dreher
Valeo Wiper System, BP 581, 78321 Le Mesnil,
Saint Denis cedex, France

P. Alliot · E. Aubry (✉)
ESSAIM, 12 rue des frères Lumière, 68093 Mulhouse cedex,
Mulhouse, France
e-mail: evelyne.aubry@uha.fr

J.-P. Lainé · L. Jézéquel
ECL, 36 Avenue Guy de Collongue, BP 163,
69131 Ecully cedex, France

Introduction

Vibratory phenomena may appear in the operation of wiper systems. These vibrations, due to flutter instabilities, are based on the coupling between the rubber blade and the glass [1] and can generate visual and audible annoyance for the driver. The phenomena appear under specific conditions: windshield moisture and cleanness, contact pressure of the rubber blade on the glass, attack angle of the wiper blade on the windshield, component stiffness, windshield curvature, etc.

For an automotive equipment supplier, the optimization at the wiper systems is top priority and motivates design engineers to find solutions to eliminate any possible wiping defects. The model which has been developed allows the prediction of the conditions of instability occurrence according to specific operational and environmental parameters influencing the system instabilities.

System Description

A conventional wiper system (Fig. 1) comprises an electric motor and a linkage mechanism which converts the rotational movement of the motor into the back and forth motion of the wiper arms [17]. The mechanical structure of the wiper blades, which is attached to the arm tips, holds the rubber blade which drains the water off the windshield [6] and [10].

Various parameters have a significant influence on the occurrence of wipe defects. There are three main categories of parameters: first, system parameters (wiper blade inertia and dimensions, stiffness, twist angles, contact pressure, geometry of the windshield [15] ...), secondly, surface and material characteristics (roughness, friction on the rubber-glass

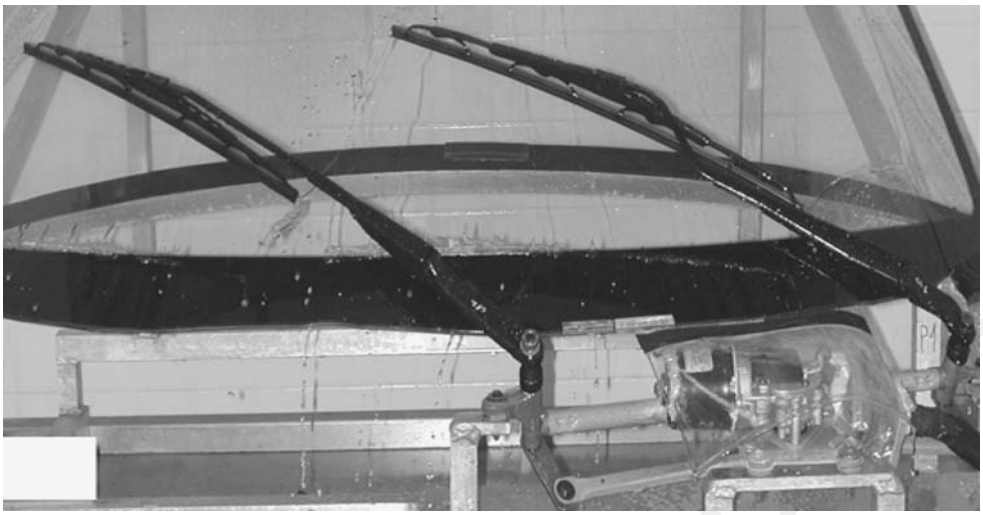

Fig. 1 Wiper system on a windshield

contact, Young modulus...) and finally, environmental and operating parameters (temperature, humidity, cleanness...).

From previous experimental tests, the present study focuses on the main parameters influencing the dynamic behaviour of the system. One of the most critical parameters for wipe quality is the attack angle which is defined as the angle between the wiper blade symmetry plane and the vector normal to the outer glass surface (Fig. 2). The windshield moisture and cleanness as well as the characteristics of the rubber blade also influence the wiping conditions. These properties are taken into account in the variation of the friction coefficient [13]. A last critical parameter is the arm tip force applied on the blade. In order to obtain a uniform contact force (expressed in N/m) under the rubber blade, it can be adjusted by a steel spring.

In a first time, the experimental wiping device will consist of a rigid blade holder with a rubber blade. This experimental device will help to characterize the first instabilities domains

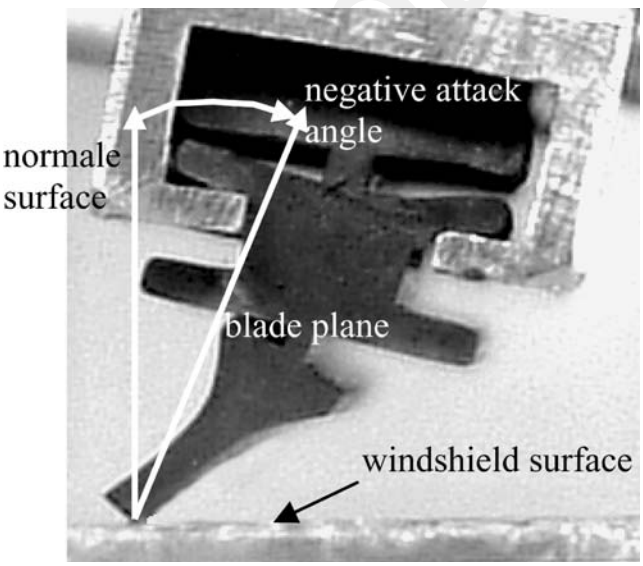

Fig. 2 Attack angle definition

of the system with a low number of degrees of freedom without taking account of the deformability of the wiper blade. Regarding previous papers [4, 5], the original contribution of this article is the consideration a new generation of flexible wiping systems.

Wiper System Modeling with Rigid Blade

Computational modelling is based on the finite elements model of the arm and rigid blade system. The finite element model comprises several degrees of freedom. The elements used here are beam elements. The rigid blade wiper system is divided into three distinct sub-systems which are the wiper arm, the rigid blade holder and the rubber blade. The dynamics of each sub-system is represented by a certain number of eigenmodes. The number of modes to be taken into account for the system is determined by the frequency range concerned.

Wiper Arm Modelling

First, a static calculation on the arm model helps to obtain the arm geometry for different attack angles. Then, from the finite element model of the arm, a Guyan Condensation [12] is performed in order to extract 30 master degrees of freedom (dof). This reduced model is validated trough comparison with a full finite element model for modal calculation. Among these 30 dof, 3 dof represent the link between the arm and the spring and 6 dof represent the link between the arm and the rigid blade holder. The resulting mass and stiffness matrices are assembled with the stiffness term of the spring. A second dof reduction is obtained through a Craig and Bampton sub-structuration method [7, 12]. In this way, the number of dof can be reduced down to 8 dof, 6 of which representing the link arm-rigid blade and 2 eigen dynamic modes (first vertical and horizontal bending modes of the

arm at 99 Hz and 79 Hz). Finally, the arm is modelled using an 8×8 mass and stiffness matrices.

Rigid Blade Holder Modelling

The first blade holder non null eigenmode is equal to 430 Hz; this eigen frequency is far from the frequency range considered in this study. So, the wiper blade is taken as a rigid body with 6 dof [4] and there is no strain energy of deformation. The coupling between the wiper arm and the rigid blade is represented by a pivot connection around the *y* axis; this link represents the sixth dof of the rigid blade holder and the five other dof are common to the wiper arm dof.

The matrix terms of the arm and the wiper blade are assembled and, finally, the mass and the stiffness matrices for the arm-rigid blade system have a rank of 9 including the additional dof due to the pivot connection, the two dynamic wiper arm dof, the three translations and the three rotations of the system. The deformation energy of the rubber blade is added to the deformation energy of the arm-rigid blade system.

Rubber Blade Modelling

Deformation model

The strain energy arising from cross-section deformation varies slowly along the blade length and so, it is computed on a per unit length basis through a bidimensional plane strain model. The rubber blade model is a non linear model, taking account of hyper elastic material behaviour, glass-rubber contact and rubber auto-contacts to describe the quasi-static behaviour. Different hypotheses can be made :

- The inertia forces associated with the rubber lip deformations are neglected;
- The longitudinal coupling of the rubber blade is neglected;
- The normal and tangential forces at the friction interface are limited by the Coulomb law $f=\mu F_N$ where μ is the dynamic friction [2, 3, 8].
- The structural damping of the rubber blade is neglected

In a first step, a quasi-static study of the rubber blade from its finite element model proves the existence of stable static solutions. The quasi-static equilibrium position is defined by the normal force F_N due to the arm spring, which crushes the rubber blade against the glass. Three solutions are possible to obtain the quasi-static stable solutions; they are shown in Fig. 3.

To ensure the stability of the non linear solution (multiple solutions), static calculations are carried out, while controlling the vertical force applied on the rubber blade and the horizontal displacement of the rubber blade-glass contact point.

From these simulation results associated with various vertical force values F_N shown in Fig. 3, and for a specific friction coefficient, the following elements can be calculated :

- The horizontal displacement u_y of the contact point related to the rigid blade holder ;
- The vertical displacement u_z of the rigid blade holder relative to the glass ;
- The tangent vertical stiffness k defined by $\frac{dF_N}{du_y}$ for a constant friction coefficient μ around the equilibrium position using a double interpolation according to two parameters (F_N,μ).

The results of the static calculation give the horizontal displacement u_y and the vertical displacement u_z. These displacements are the difference between the reference position and the initial position. The reference position is defined as: "rubber blade is not deformed and is in contact with the glass". From u_y and u_z, the values of parameters a and b are obtained so that $a = a_0 + u_y$, where a_o corresponds to the horizontal distance between the contact point of the non deformed rubber blade with the glass and the hook point, and u_y is the horizontal displacement of the con-

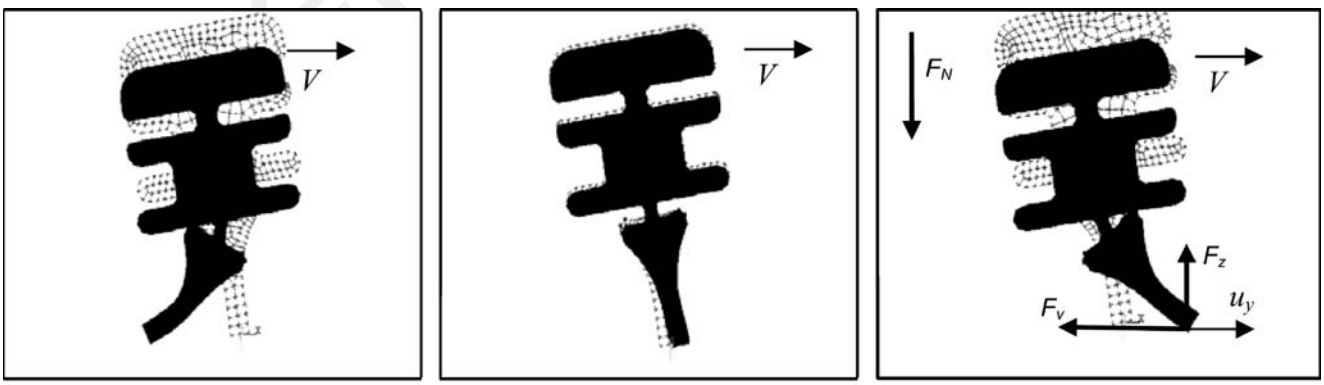

Fig. 3 Rubber blade positions

tact point compared to this reference position a_o. In the same way, $b = b_0 + u_z$, where b is the vertical displacement.

The tangent stiffness k is calculated using a double interpolation according to two parameters of the quasi-static simulation results. Indeed, in order to obtain better accuracy for the k calculation, a first interpolation is performed with the applied force, followed by a second interpolation with the friction coefficient μ. For each kind of solution, there are potentially stable quasi-static solutions and potentially unstable quasi-static solutions (negative stiffness) depending on the sign of k. Thus, for solution 1, $k>0$ indicates quasi-static stable solutions; same results are obtained for solution 3. However, for solution 2, k can be negative or positive, so there are stable or unstable quasi-static solutions. Parameters a, b and k, characteristic of the rubber blade, allow the calculation of its stiffness matrix and represent the input parameters for the dynamic study.

Rubber blade model

The forces due to the rubber blade deformations are integrated along the blade and small displacements around the static equilibrium position will be considered. This position depends on the spring stiffness, the friction coefficient and the rubber blade stiffness k. So, the generalized force vector $\boldsymbol{F}$ of the glass on the rubber blade will depend linearly on the generalized displacement vector $\boldsymbol{q}$ of the wiper blade. This will lead to the linearized stiffness matrix which depends on the friction coefficient and the geometry of the static deformation of the rubber blade.

This stiffness matrix of the rubber blade K_{dl} can be written as

$$\boldsymbol{F} = [K_{\mathrm{dl}}]_q \tag{1}$$

with $\boldsymbol{F}^T = (F_X\, F_Y\, F_Z\, M_X\, M_Y\, M_Z)$ where F represents the forces and M the torque forces and the generalized displacement vector $\boldsymbol{q}^T = (U_X\, U_Y\, U_Z\, \theta_X\, \theta_Y\, \theta_Z)$ where U_X, U_Y and U_Z are the translation displacements and θ_X, θ_Y, θ_Z are the rotation angles of the hook point between the arm and the rigid blade.

These displacements

$$\overrightarrow{u}_M = \begin{pmatrix} U_X \\ U_Y \\ U_Z \end{pmatrix} + \begin{pmatrix} \theta_X \\ \theta_Y \\ \theta_Z \end{pmatrix} \wedge \begin{pmatrix} x \\ a \\ b \end{pmatrix} \tag{2}$$

along the rigid blade are expressed at the link point O between the arm and the rigid blade; a and b are defined by $a = a_0 + u_y$ and $b = b_0 + u_z$.

In these equations, the contact conditions of the rubber blade against the glass are taken into account.

Flutter Instability Study

The calculation of the mass and stiffness matrices corresponding to the arm and rigid blade system gives the equation system

$$[\boldsymbol{M}_F]\left[\ddot{Q}\right] + [\boldsymbol{K}_F][Q] = 0 \tag{3}$$

linearized around the equilibrium position, taking account of small displacements.

$[\mathbf{M}_F]$ is the assembled mass matrix and $[\mathbf{K}_F]$ is the assembled stiffness matrix, which is non symmetric due to friction coupling terms.

The generalized vector $\boldsymbol{Q}$ is given by $Q^T = (d_1\, d_2\, U_X\, U_Y\, U_Z\, \theta_X\, \theta_{Y\mathrm{ar}}\, \theta_Z\, \theta_{Y\mathrm{wb}})$ where d_1 and d_2 represent the first two dynamic eigenmodes of the arm; $\theta_{Y\mathrm{ar}}$ is the arm rotation and $\theta_{Y\mathrm{wb}}$ is the blade rotation around y axis at the hook point.

The dynamic stability is tested in the neighbourhood of each realistic equilibrium point. According to the set of input parameters (arm force, friction coefficient and various attack

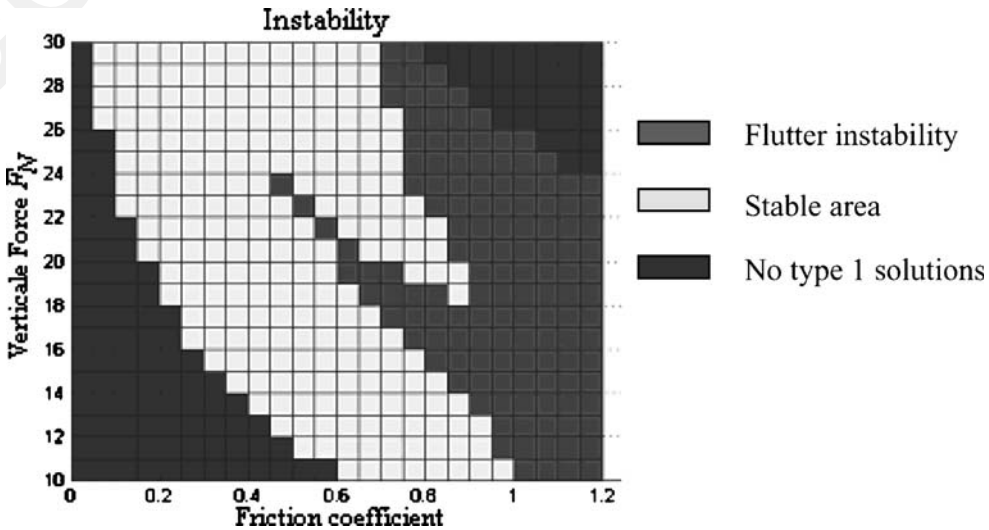

Fig. 4 Instability areas in the rigid blade system for solution 1 with an attack angle of 15°

angles), the eigenvectors and eigenvalues of the equation system are calculated so as to detect flutter instability domains [14, 18].

The instability areas for solution 1 with an attack angle of 15° are examined in Fig. 4, according to (F_N,μ). The various graphs obtained with such a study for various attack angles clearly show that instability areas appear for attack angles higher than 9°, and the system remains stable for attack angles lower than 9°. So, the attack angle has a strong influence on the occurrence of instabilities.

The wiper system stability is tested by studying the eigenvalue evolution versus the friction coefficient μ for given attack angles and arm forces. The real part and the imaginary part of the solution of the equation system will be considered here.

Figure 5 shows an example with an attack angle of 15°, and an arm force of 15 N/m considering a friction coefficient from 0 to 1.6.

In this figure, two different areas can be observed :

- First area : $0<\mu<0.8$: stable area (eigenvalue with null real part);
- Second area: $\mu>0.8$: unstable area (eigenvalue with positive real part and non null imaginary part); flutter instability with a Hopf bifurcation at $\mu=0.8$ with a point of coalescence of two modes [11, 16]. So, there is a coupling between modes 2 and 3, which creates the instability.

In this case, the flutter instability appears for a friction coefficient $\mu>0.8$ with a frequency of 25 Hz. So, this first theoretical model allows the simulation of the behaviour of an experimental wiping system device with a rigid blade holder on a flat glass surface.

Rigid Model Validation

Various experimental tests were carried out on a flat glass bench fitted with accelerometers and a torque sensor. The accelerometers detect the acceleration and the frequencies of the system. The torque sensor helps to determine the friction coefficient between the glass surface and the rubber blade. These tests highlight reveal the system instabilities according to the arm force, the attack angle and the friction coefficient.

The experimental results obtained show frequency instabilities at 22 Hz. The theoretical model predicts flutter instabilities at 25 Hz. Moreover, it can be noticed that the theoretical unstable areas correspond to the experimental unstable areas. Finally, these tests help to validate this first theoretical model with a very good correlation between the theoretical and experimental results. This first validation shows encouraging results which will lead to the second step of flexible wiper system modeling.

Flexible Blade Wiper System Modelling

Modeling

The rubber blade with steel reinforcement behaves like a flexible composite beam. For bending strain energy, the deformation of the cross section is neglected. Strain energy

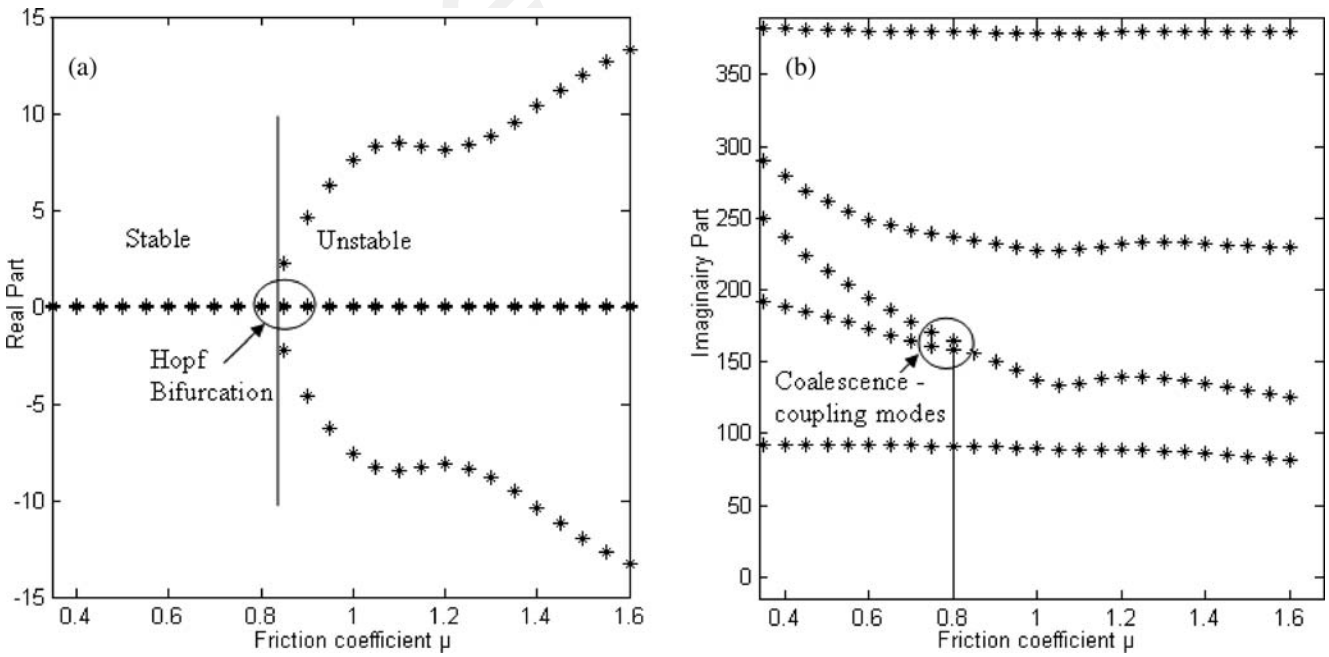

Fig. 5 Real part (**a**) and Imaginary part (**b**) of the rigid blade system (F=15 N/m and attack angle=15°)

associated with cross-section deformation is computed on a per unit length basis through a plane strain model. The final linearized model is a beam on an elastic foundation.

The validated rigid blade system model is used as the basis for the flexible blade system model. Indeed, the wiper arm modelling and the rubber blade modelling are conserved from the rigid blade system modelling. The main difference is the deformability of the wiper blade. So, the horizontal and vertical flexion of the wiper blade must be modelled. This particularity adds several dof to the final equation system. The method used to model the wiper arm is the same as described in "Wiper Arm Modelling" section. In particular, the dynamic behaviour is described using the same modal synthesis method.

A new wiper blade mass matrix is calculated taking account of the deformation energy due to the flexions [5]. Moreover, in the rigid blade case, the stiffness matrix is null because the wiper blade is considered as a rigid beam, but considering the flexible blade system, this matrix is included in the model.

The wiper blade deformations for bending directions are taken into account through a Rayleigh–Ritz procedure [9, 18]:

$$\begin{aligned}\phi_{Yi} &= \sum_i \lambda_{Yi} \frac{x^{i+1}}{(L/2)^{i+1}} \text{ and } \phi_{Zi} \\ &= \sum_i \lambda_{Zi} \frac{x^{i+1}}{(L/2)^{i+1}} \text{ with } \frac{x^{i+1}}{(L/2)^{i+1}} \text{ is a trial function}\end{aligned} \tag{4}$$

λ_{Yi} and λ_{Zi} are the generalized displacements in the Y and Z directions, and L is the length of the wiper blade.

To obtain the mass matrix of the flexible wiper blade, its kinetic energy in its centre of inertia must be calculated. The kinetic energy is expressed as

$$\mathrm{Ec} = \frac{1}{2}\int_{-L/2}^{L/2} (\rho \mathrm{d}x)\left(\dot{u}_{GX}^2 + \dot{u}_{GY}^2 + \dot{u}_{GZ}^2\right) \tag{5}$$

where ρ is the mass per unit length and u_{Gx}, u_{Gy} and u_{Gz} are the centre of inertia displacements expressed as

$$\overrightarrow{u}_G = \begin{pmatrix} U_X \\ U_Y \\ U_Z \end{pmatrix} + \begin{pmatrix} \theta_X \\ \theta_Y \\ \theta_Z \end{pmatrix} \wedge \begin{pmatrix} x \\ a_G \\ b_G \end{pmatrix} + \begin{pmatrix} 0 \\ \phi_{Y1} \cdots \phi_{Y4} \\ \phi_{Z1} \cdots \phi_{Z4} \end{pmatrix} \tag{6}$$

where a_G and b_G are the centre of inertia coordinates in R,

U_X, U_Y and U_Z are the translation displacements and θ_X, θ_Y, θ_Z the rotation angles of the hook point.

The substitution of the equation (5) for equation (4) gives

$$\mathrm{Ec} = \frac{1}{2} q^{'T} [M_d] q^{'} \tag{7}$$

where $\mathbf{M}_d$ is the mass matrix of the flexible wiper blade and $\boldsymbol{q}^T$ the generalized vector displacement:

$$\boldsymbol{q}^T = \left(U_x\, U_y\, U_Z\, \theta_X\, \theta_Y\, \theta_Z\, \lambda_{Y1}\, \lambda_{Z1}\, \ldots \lambda_{Y4}\, \lambda_{Z4}\right)$$

The stiffness matrix of the wiper blade depends on the bending rigidity EI which is updated from the results of the modal analysis of the wiper blade alone. The strain energy is expressed as:

$$\mathrm{Ep} = \frac{1}{2}\int_{-L/2}^{L/2} EI\left(\ddot{\phi}_y(x)\right)^2 + EI\left(\ddot{\phi}_z(x)\right)^2 \mathrm{d}x \tag{8}$$

So,

$$\mathrm{Ep} = \frac{1}{2}\boldsymbol{q}^T [\mathbf{K}_d] \boldsymbol{q} \tag{9}$$

where $\mathbf{K}_d$ is the stiffness matrix of the flexible wiper blade.

The deformation model of the straight cross section due to the crushing of the rubber blade against the glass is exactly the same as in "Rubber Blade Modelling" section. On the other hand, in the case of the flexible wiper system, a second source of deformation energy due to the flexion movements is taken into account. However, the stiffness matrix of the rubber blade including the flexible deformation in the Y and Z directions must be calculated.

So, small displacements dx around point M will be considered.

The displacements are expressed at the link point O between the arm and the wiper blade:

$$\overrightarrow{u}_M = \begin{pmatrix} U_X \\ U_Y \\ U_Z \end{pmatrix} + \begin{pmatrix} \theta_X \\ \theta_Y \\ \theta_Z \end{pmatrix} \wedge \begin{pmatrix} x \\ a \\ b \end{pmatrix} + \begin{pmatrix} 0 \\ \phi_{Y1} \ldots \phi_{Y4} \\ \phi_{Z1} \ldots \phi_{Z4} \end{pmatrix} a \tag{10}$$

where $\overrightarrow{OM} = \begin{vmatrix} x \\ a \\ b \end{vmatrix}$, so that $a = a_0 + u_y$ and $b = b_0 + u_z$

So, the stiffness matrix of the rubber blade can be expressed as

$$F = [\mathbf{K}_{\mathrm{dl}}] \boldsymbol{q} \tag{11}$$

with $\mathbf{K}_{\mathrm{dl}}$ the stiffness matrix of the rubber blade, $\boldsymbol{q}$ the generalized displacement vector $\boldsymbol{q}^T = \left(U_x\, U_y\, U_Z\, \theta_X\, \theta_Y\, \theta_Z\, \lambda_{Y1}\, \lambda_{Z1}\, \ldots \lambda_{Y4}\, \lambda_{Z4}\right)$

The generalized force vector is $F^T = \left(F_x\, F_y\, F_Z\, M_X\, M_Y\, M_Z\, F_{\mathrm{d}Y1}\, F_{\mathrm{d}Z1} \ldots F_{\mathrm{d}Y4}\, F_{\mathrm{d}Z4}\right)$ with F the forces and M the torque value defined as :

$$\mathrm{d}F = \begin{vmatrix} \mathrm{d}F_X \\ \mathrm{d}F_Y \\ \mathrm{d}F_Z \end{vmatrix} = \begin{vmatrix} 0 \\ \mu \mathrm{d}F_Z \\ -k u_Z \mathrm{d}x \end{vmatrix} \tag{12}$$

$$\mathrm{d}\vec{M} = O\vec{M} \wedge \mathrm{d}\vec{F} = \begin{pmatrix} x \\ a \\ b \end{pmatrix} \wedge \begin{pmatrix} \mathrm{d}F_X \\ \mathrm{d}F_Y \\ \mathrm{d}F_Z \end{pmatrix} = \begin{pmatrix} \mathrm{d}\vec{M}_X \\ \mathrm{d}\vec{M}_Y \\ \mathrm{d}\vec{M}_Z \end{pmatrix} \tag{13}$$

Parameter k is the tangent stiffness defined in "Rubber Blade Modelling" section. Moreover,

$$F_{\mathrm{d}yi} = -\int_{-L/2}^{L/2} \phi_{yi}\mathrm{d}F_{yi} \text{ and } F_{\mathrm{d}zi} = -\int_{-L/2}^{L/2} \phi_{zi}\mathrm{d}F_{zi} \tag{14}$$

Flutter Instabilities Study

The stability study for the flexible blade system is the same study as for the rigid blade system. The calculation of the final mass and stiffness matrices corresponding to the arm and flexible blade system gives

$$[\mathbf{M}_F]\left[\ddot{Q}\right] + [\mathbf{K}_F][\boldsymbol{Q}] = 0 \tag{3}$$

but in the case of the flexible blade system, the generalized vector $\boldsymbol{Q}$ becomes

$$\boldsymbol{Q}^T = (d_1\, d_2\, U_X\, U_Y\, U_Z\, \theta_X\, \theta_{Y\mathrm{ar}}\, \theta_Z\, \theta_{Y\mathrm{wb}}\, \lambda_{Y1}\, \lambda_{Z1}\, \ldots \lambda_{Y4})$$

with d_1 and d_2 representing the two first dynamic eigen modes of the arm.

Moreover, $\theta_{Y\mathrm{ar}}$ is the arm rotation and $\theta_{Y\mathrm{wb}}$ is the blade rotation around the y axis at the hook point. This final system has 17 dof. Dynamic stability is tested in the neighbourhood of each realistic equilibrium point. According to the set of input parameters (arm force, friction coefficient and various attack angles) the eigenvectors and eigenvalues of the equation system are calculated in order to detect the flutter instabilities regions (cf Section 3.4.1).

The instability areas for solution 1 with an attack angle of 15° are examined in Fig. 6 according to ($F_{\mathrm{N},\mu}$). An example with an attack angle of 15°, an arm force of 15 N/m considering a friction coefficient μ from 0 to 2 shows the eigenmode evolution of the flexible blade system (Fig. 7). Two different areas can be observed :

- First area : $\mu<\mu 1$: stable area (eigenvalue with null real part),
- Second area: $\mu>\mu 1$: unstable area (eigenvalue with positive real part and non null imaginary part), flutter instability with a Hopf bifurcation at $\mu=\mu 1$ with a point of coalescence of two modes [11, 16].

So, in this case, the coupling mode creates the flutter instability for $\mu>\mu 1$ with frequency f=61 Hz. Moreover, whatever the set of parameters used in the model, frequency instabilities are obtained around 60 Hz.

Validation

Various series of experimental tests, varying the arm force and the attack angle, were carried out to show the instability phenomenon, such as chatter.

Arm Force: [12 15 18] N/m (nominal pressure pre-defined by the vertebra shape);

Attack angle: [7 10 12 15] degrees.

Accelerometers were placed on the flexible wiper system for normal measurements to the wiper blade plane (rising of the wiper blade in Z) and tangential measurements to the wiper blade plane (bending of the wiper blade in Y). Par-

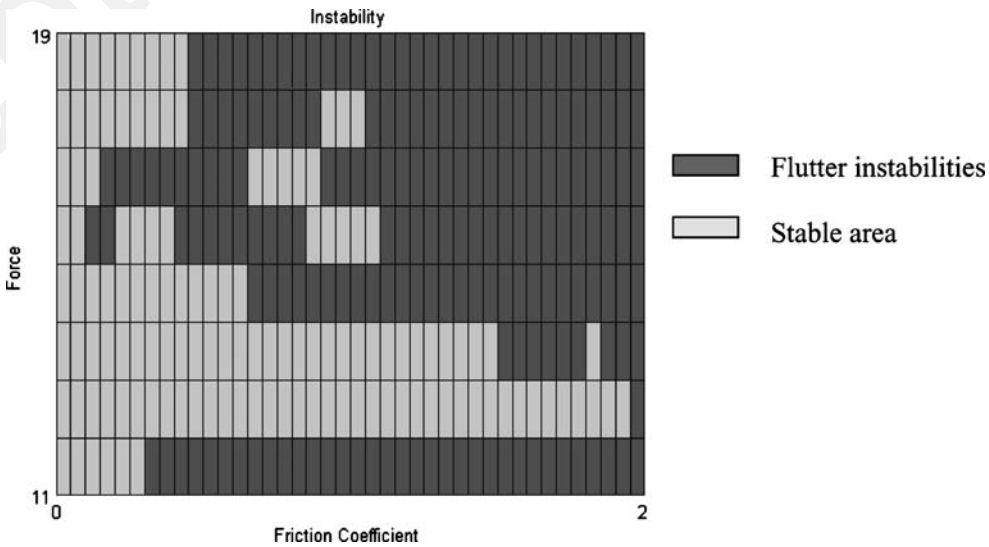

Fig. 6 Instability areas in the flexible blade system for solution 1 for an attack angle of 15°

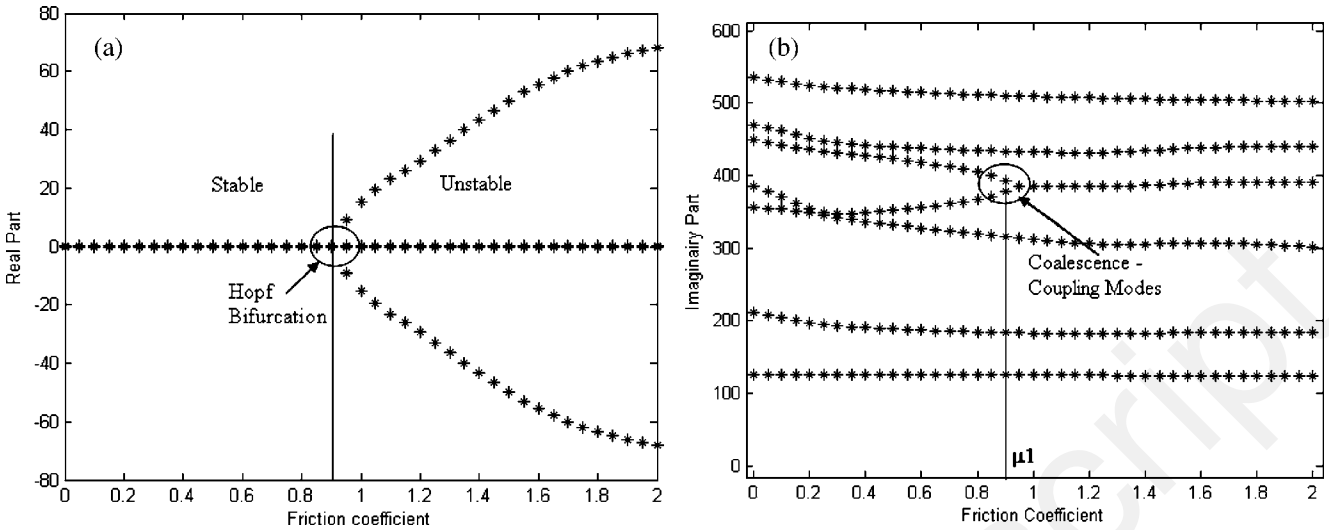

Fig. 7 Real (**a**) and Imaginary (**b**) parts of the flexible blade system (F=15 N/m and attack angle=15°)

ticular care was taken to ensure that the additional mass of the accelerometers did not affect the structural frequencies.

Friction between the rubber lip and the glass surface depends on humidity. The mean friction coefficient is determined through the total resistive torque on the wiper shaft. For each test configuration (applied pressure, attack angle), the mean friction coefficient was calculated from the ratio between normal and tangential force.

Results

Friction coefficient μ obtained with the torque sensor:

- Wet glass, $0.2<\mu<0.4$;
- Tacky glass, $\mu>1.2$;
- Dry glass, $0.8<\mu<1$.

The graphs [Fig. 8(a) and (b)] show the auto-spectrum in the perpendicular direction Z.

Figure 8(a) presents the results without instabilities where experimental vibratory frequencies appear. The eigen frequencies of the structure were calculated by the model and correspond to the experimental frequencies (Table 1). The experimental eigen frequencies do not appear distinctly due to their low vibratory level. These eigen frequencies are low frequencies and can be overlapped with electromagnetic (50 Hz and harmonics) and vibratory background noises. The system structural modes can vary due to the friction coefficient coupling.

Figure 8(b) shows instabilities with a high amplitude obtained at the frequency of 62.5 Hz. The comparison of the two figures shows that, when instabilities appear, the level of the spectra amplitude is at least 100 times higher than it is when the system is stable (the vertical displacement amplitude can reach 0.4 mm). The various results obtained show a variation in the amplitude spectra along the blade.

Generally, the level of the spectra amplitude is higher for tacky glass surface than for wet glass. Moreover, the insta-

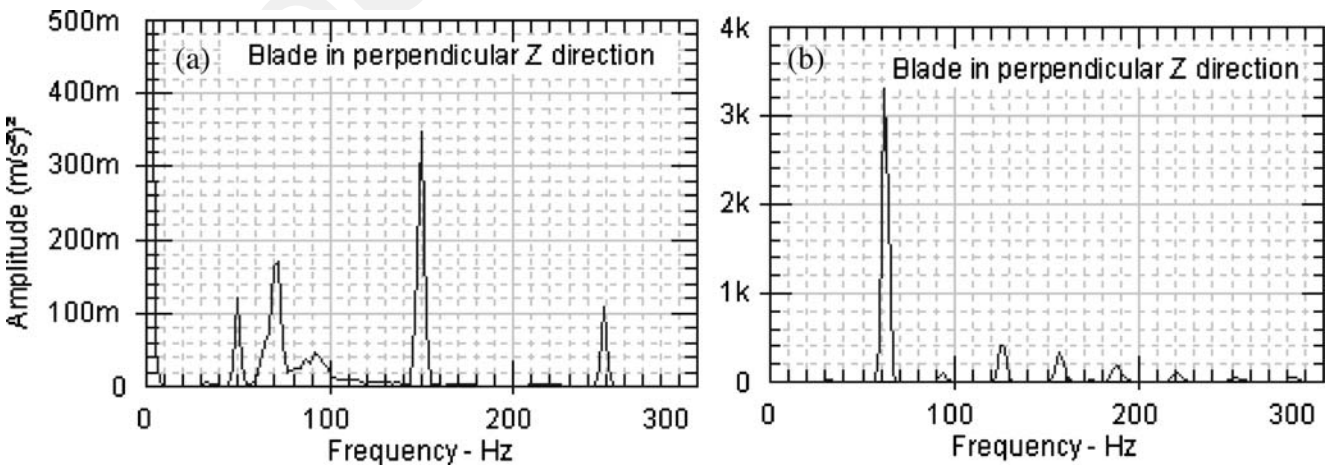

Fig. 8 (**a**) Auto spectrum without chatter (F=15 N/m, Attack angle=15° and μ=0.3); (**b**) Auto spectrum with chatter (F=15 N/m, Attack angle=15° and μ=2)

Table 1 Comparison of the eigen frequencies

Theoretical eigen frequencies (Hz)	18	32	55	63	67	75	124	133
Experimental eigen frequencies (Hz)		32.5	50			72.5	95	150

bilities level can vary according to the nominal pressure applied to the system.

These tests reveal a sensitivity of the experimental results versus the environmental conditions and the difficult control of number of experimental parameters, such as the friction coefficient. Unlike the fixed input parameter force, the friction coefficient is a measurement result, so the entire range of the friction coefficient is difficult to explore.

Correlation with the Theoretical Model

The theoretical model is validated by the comparison of the theoretical and experimental frequencies and instability areas. First, the theoretical model shows an unstable mode at 60 Hz (Fig. 7) very close to the experimental value 62.5 Hz. When this instability occurs, the displacement of the system is characterized by the corresponding eigenvector. This modal shape can be described in terms of modal displacement amplitudes and helps to understand the phenomena and to deduce the displacement of the system. It is interesting to observe the level of displacement along the wiper blade.

- Blade Middle : U_Z=8.74 10^{-5}
- Blade tip : $U_z + \lambda_{Z1} + \frac{1}{2}\theta_{Y\mathrm{wb}} = 2.0210^{-4}$
- Blade heel : $U_Z + \lambda_{Z1} + \frac{1}{2}\theta_{Y\mathrm{wb}} = 3.1610^{-4}$

So, the amplitude level of the heel of the blade is higher than the amplitude level of the tip of the blade and the middle of the blade according to the results obtained through the theoretical analysis.

Table 2 Validation table

	15°	12°	10°	7°	Total
Good correlation	16	19	21	12	68
Poor correlation	2	3	1	3	9
Rate of correlation(%)	88	86	95	80	88

When the instability appears, the experimental results shows that the amplitude level of the heel of the blade is higher than the amplitude level of the tip of the blade and the middle of the blade. So, there is a theoretical structural movement compatible with the experimental movement.

The theoretical and experimental chart (Fig. 9) presents the instability areas when the blade is in a wiping situation. Situation 1 is likely to appear during wiping. Solutions 2 and 3 will tend toward solution 1.

Validation Criteria:

- Instability peak at frequency f ;
- Instability level in the range of 1,000 $(m/s^2)^2$;
- Instabilities with visual mark on the glass and noise.

Validation Table This validation table (Table 2) is established according to the criteria defined above. So, the rate of correlation between the experimental results and the theoretical results is 88%.

Conclusion

The theoretical model developed for the new generation of flexible wiper systems allows a highly satisfactory predictive approach to the instabilities phenomenon. Over a hundred experimental tests led to a correlation at 88% between the model and the experimentation.

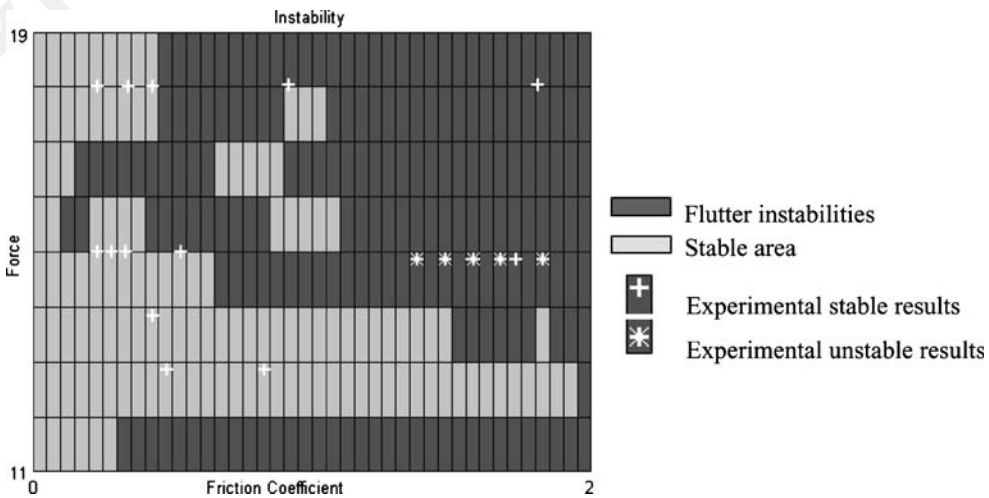

Fig. 9 Instability areas in the flexible blade system for wiping solution 1 with an attack angle of 15°

It is essential to note that the experimental results are sensitive to the environmental conditions. A number of parameters, such as the friction coefficient between the rubber blade and the glass which is a measurement result, are not easy to control.

The present model, validated by experimental tests, is a new tool that will help designers to adopt the optimum set of parameters for a robust wiper system in terms of resistance to dynamic instabilities.

References

1. Begout M (1979) Les problèmes liés au frottement élastomère-verre dans l'automobile. Mémoire de thèse, Université Paul Sabatier Toulouse, 2206.
2. Boudot JP (1995) Modélisation des bruits de freinage des véhicules industriels. Mémoire de thèse, Ecole Centrale Lyon, 95–08.
3. Chambrette P (1990) Stabilité des systèmes dynamiques avec frottement sec: application au crissement des freins à disque. Mémoire de thèse, Ecole Centrale Lyon, 91–48.
4. Chevennement-Roux C, Grenouillat R, Dreher T, Alliot P, Aubry E, Laine JP, Jézéquel L (2004) Mise en évidence des instabilités d'un système d'essuyage par analyse vibratoire-corrélation avec un modèle théorique, XIV^{e} Colloque Vibrations Chocs et Bruit, Ecole Centrale Lyon.
5. Chevennement-Roux C, Grenouillat R, Dreher T, Alliot P, Aubry E, Laine JP, Jézéquel L (2005) Wiper systems with flexible structures-instabilities analysis and correlation with a theoretical model, SAE, Article 2005-01-2375.
6. Codfert V (1997) Modélisation globale d'un système d'essuyage, Mémoire de thèse, Université des Sciences et Technologies de Lille.
7. Craig RR, Bampton MCC (1968) Coupling of substructures for dynamic analysis. AIAA J 6(7):1313–1319.
8. Earles SWE, Badi MNM (1984) Oscillatory instabilities generated in a double pin-disc undamped system : a mechanism of disc-brake squeal. Proc Inst Mech Eng 198C(4):43–50.
9. Géradin M, Rixen D (1993) Théorie des vibrations-application à la dynamique des structures, Masson.
10. Grenouillat R (2001) Etude des défauts d'essuyage: application à l'analyse prédictive, Mémoire de thèse, Ecole Centrale de Lyon.
11. Guckenheimer J, Holmes P (1986) Nonlinear oscillations, dynamical systems, and bifurcations of vector fields, Springer, Berlin Heidelberg New York.
12. Imbert JF (1995) Analyse des structures par éléments finis, Cepadues Editions, ISBN 2.85.428.273.6.
13. Koenen A (1998) Rapport de synthèse sur le frottement du caoutchouc, Rapport n°03 98 186, Laboratoire de Tribologie VSE, La Verrière.
14. Moirot F, Guyen QSN (2000) Brake squeal: a problem of flutter instability of the steady sliding solution? Arch Mech 52(4–5): 645–661.
15. Muradore F, Dreher T, Jan S (2004) Windshield shape optimization using neural network, SAE Article.
16. Nayfeh AH, Balachandran B (1995) Applied nonlinear dynamics: analytical, computational and experimental methods. Wiley, New York.
17. Okura S, Sekigushi T (2000) Dynamic analysis of blade reversal behavior in a windshield wiper system, SAE Papers, 2000-01-0127.
18. Sinou JJ (2002) Synthèse non-linéaire des systèmes vibrants. Application aux systèmes de freinage, Mémoire de thèse, Ecole Centrale de Lyon.